Journal of Cosmology and Astroparticle Physics
An IOP and SISSA journal

Received: March 4, 2025
Revised: August 2, 2025
Accepted: August 21, 2025
Published: October 14, 2025

# On the impacts of halo model implementations in Sunyaev-Zeldovich cross-correlation analyses

**Chad Popik**,[a] **Nicholas Battaglia**,[a,b] **Aleksandra Kusiak**,[c,d] **Boris Bolliet**[d,e] **and J. Colin Hill**[f]

[a] *Department of Astronomy, Cornell University, Ithaca, NY 14853, U.S.A.*
[b] *Université Paris Cité, CNRS, Astroparticule et Cosmologie, F-75013 Paris, France*
[c] *Institute of Astronomy, University of Cambridge, Cambridge, CB3 0HA, U.K.*
[d] *Kavli Institute for Cosmology, University of Cambridge, Cambridge CB3 0HA, U.K.*
[e] *DAMTP, Centre for Mathematical Sciences, Cambridge CB3 0WA, U.K.*
[f] *Department of Physics, Columbia University, New York, NY 10027, U.S.A.*
*E-mail:* cp527@cornell.edu, nb572@cornell.edu, ak2628@cam.ac.uk, bb667@cam.ac.uk, jch2200@columbia.edu

Abstract: Statistical studies of the circumgalactic medium (CGM) using Sunyaev-Zeldovich (SZ) observations offer a promising method of studying the gas properties of galaxies and the astrophysics that govern their evolution. Forward modeling profiles from theory and simulations allows them to be refined directly off of data, but there are currently significant differences between the thermal SZ (tSZ) observations of the CGM and the predicted tSZ signal. While these discrepancies could be real, they could also be the result of decisions in the forward modeling used to build statistical measures from theory. In order to see effects of this, we compare an analysis utilizing halo occupancy distributions (HODs) implemented in halo models to simulate the galaxy distribution against previous studies, which weighted their results to match the CMASS galaxy sample, which contains nearly one million galaxies, mainly centrals of group-sized halos, selected for relatively uniform stellar mass across redshifts between $0.4 < z < 0.7$. We review some of the implementation differences that can account for changes, such as miscentering, one-halo/two-halo cutoff radii, and mass ranges, all of which will need to be given the proper attention in future high-signal-to-noise studies. We find that our more thorough model predicts a signal with a 33% improved fit than the one from previous studies on the exact same sample. Additionally, we find that modifications that change the satellite fraction even by just a few percent, such as editing the halo mass range and certain HOD parameters, result in strong changes in the final signal. Although significant, this discrepancy from the modeling choices is not large enough to completely account for the existing disagreements between simulations and measurements.

Keywords: redshift surveys, Sunyaev-Zeldovich effect, galaxy clusters, feedback in galaxies

ArXiv ePrint: 2502.13291



https://doi.org/10.1088/1475-7516/2025/10/051

JCAP10(2025)051

## Contents



## 1 Introduction

Galaxy formation and evolution are subjects of major interest in modern-day astronomy and cosmology, with a multitude of open questions. Among them is the observed inefficiency of star formation [1–3], the missing baryon problem [1, 4–6], and the role that feedback from supernovae (SN) and active galactic nuclei (AGN) plays in their host galaxies [7–13].

A vital component for studying these questions is the circumgalactic medium (CGM), the region of diffuse ionized gas that surrounds a galaxy [14]. This region is known to have significant interaction with galaxies in the form of turbulence flows and thermodynamic exchanges [15–17]. The CGM has been observed directly through absorption lines [18–27], and improvements in observation technology have led to studies on emission lines [28–34]. Furthermore, there have been many studies using simulations to understand the astrophysics involved in the CGM [35–39].

Within the past decade, large galaxy redshifts surveys such as the Sloan Digital Sky Survey's (SDSS) Baryon Oscillation Spectroscopic Survey (BOSS) [e.g., 40] paired with high resolution wide field observations such as the tSZ, lensing [e.g., 41], and X-rays [e.g., 42] opened the door to statistical studies of galaxies properties. With datasets including hundreds of thousands or millions of galaxies, researchers can extract general properties about the CGM that surrounds galaxies which then can be used to guide theoretical modeling and simulations. Cross-correlating observations with overlapping galaxies catalogs serves as a promising method to do this, by creating high signal-to-noise measurements of survey-averaged galaxy properties.

One such observation is the thermal Sunyaev-Zeldovich (tSZ) effect, a secondary anisotropy of the Cosmic Microwave Background (CMB) caused by the inverse-Compton scattering of CMB photons off of electrons in hot regions of space [43, 44]. The tSZ effect



JCAP10(2025)051

manifests as temperature fluctuations of $\Delta T_{\rm tsz}/T_{\rm CMB} \sim 10^{-5}$, and can be described as follows:

$$\frac{\Delta T(\nu)}{T_{\rm CMB}} = f(\nu) y(\theta)\,, \tag{1.1}$$

where $\Delta T(\nu)$ is the temperature deviation caused by the tSZ effect at a frequency $\nu$, $T_{\rm CMB} = 2.725$ K is the temperature of the CMB, and $f(\nu) = x\coth(x/2) - 4$ is the spectral function where $x = \frac{h\nu}{k_B T_{\rm CMB}}$, where $h$ and $k_B$ are Planck and Boltzmann constants, respectively. The final term is the Compton-$y$ parameter at angular size $\theta$, defined as the integral of the electron pressure over the line of sight:

$$y(\theta) = \frac{\sigma_T}{m_e c^2} \int_{\rm LOS} P_e\Big(\sqrt{l^2 + d_A^2(z)|\theta|^2}\Big) dl\,, \tag{1.2}$$

where $\sigma_T$ is the Thompson cross-section, $m_e$ is the electron rest mass, $c$ is the speed of light, $P_e$ is the electron pressure, $l$ is the line of sight distance, $d_A$ is the angular diameter distance at redshift $z$.

Maps of the tSZ therefore can be used as a probe of thermal energy of the matter distribution in the universe, and statistically averaging these measurements with galaxies would then yield an average pressure profile for that catalog of galaxies. Such analyses have been carried out with many different experiments before [45–52], using one of two nominal methods. The first involves taking cuts of the tSZ map reprojected to center each galaxy in the survey, and stacking these to get a mean signal of the survey galaxies. The second is creating map of the galaxy overdensity and cross-correlating it with the tSZ map to get a galaxy-$y$ cross-spectrum, which corresponds to a survey-averaged tSZ profile (but in Fourier space). Both methods can be used to study the strength and shape of the tSZ signal, but each analysis has its own associated methodologies and systematics which must be accounted for when attempting comparisons between their results.

The goal of making such measurements is to then be able to extract astrophysical and potentially cosmological information, by forward modeling analytic/semi-analytic models to produce a predicted signal that can then be fit to the results from data. Constructing average measurements requires a solid understanding of the target sample, such as its redshift and mass distribution, as well as an accurate implementation in the model.

From the ΛCDM model of cosmology, galaxies and galaxy clusters are seeded within dark matter halos, and so these analyses often employ halo models [53–55], which calculate the distribution of matter in the universe and the evolution of structure using dark matter halos as the building blocks of large scale structure [46, 48, 56]. The distribution of galaxies can then be extrapolated from the halo model distributions, in a way adapted to the galaxy survey being analysed.

Using emulators built off simulations in place of (semi)analytic models offers an opportunity to directly connect real data to the implementation of astrophysics in simulations, and possibly constrain the strength of thermodyanmic effects. Previous attempts to perform this have found that the predicted modelling from simulations significantly underestimates the signal in data [57]. However, as noted earlier, there is significant variation between forward modeling procedures, which could introduce systematics and alterations in the results that would be an effect of methodology, instead of inherent different between simulations and



JCAP10(2025)051

measurements. In [58] the authors investigated the importance of modeling the galaxy sample, such as different sample selections in the simulation and different fitting models. Ref. [59] continued this work, looking into systematics in the forward modeling process and finding minimal changes in altering the projection of 3D pressure profiles to observable signals. This study seeks to extend these analyses to the implementation halo models, specifically their use of Halo Occupancy Distributions (HODs) [54, 55, 60, 61] to populate dark matter halos with central and satellite galaxies. This is a process used in the modelling of galaxy-$y$ cross-spectra analyses, but not in stacking analyses such as the previous two papers and [57], and therefore we compare the results of this analyses on the same data but using HOD modelling to see if the difference in modelling could be responsible for the discrepancies between measurements and simulations. Additionally, we also examine the effect of miscentering, which has been utilized in lensing analyses but has not yet been examined for tSZ cross-correlation studies [62].

This paper is organized as follows: in section 2, we detail the methodology of forwarding a theoretical pressure profile to an observable average tSZ signal using a halo model (with HOD) to recreate the statistical measure. The starting profiles and projection functions used in 2.1 and 2.5, respectively, we seek to keep consistent between the two analyses, highlighting the differences in methodology arisen form the HOD and halo model details in 2.2 and 2.3, respectively. In section 3 we examine the effect of the HOD as well the effects of miscentering. Section 3.2 explores the HOD parameters we used and their impact on the tSZ signal. We then discuss our conclusions and the implications our findings have on future analyses of upcoming data in section 4.

## 2 Theory and methodology

The SZ measurements used throughout this work by [50] use the CMASS sample which is characterized as Luminous Red Galaxies (LRGs, [63]), which were selected to be central galaxies of halos with masses $M_h < 10^{14} M_\odot$; studies have estimated $\geq 90\%$ of the sample to agree with this classification [64]. Galaxies in this survey occupy a redshift range of $0.4 < z < 0.7$ with a median value of $z = 0.55$, and stellar mass and halo mass ranges of $10.71 < \log_{10}(M_\star/M_\odot) < 11.72$ and $12.12 < \log_{10}(M_h/M_\odot) < 13.98$, respectively.

We compare our methodology of using an HOD to generate a sample mass-average 3D pressure profile to the methodology [57] and [58] (used to analyze the SZ measurements from [50]), which involved taking a weighted average of 3D pressure profiles using a halo distribution obtained from galaxy stellar mass estimates and stellar-halo mass relations. To be consistency regarding all other components of the forward model we use identical pressure and density models, as described in more detail in 2.1. We then use an identical projection and beam convolution model, as described in more detail in 2.5, to predict an observed tSZ signal at 150 GHz from both methodologies.

### 2.1 Pressure and density models

We use a generalized Navarro-Frenk-White profile (GNFW), proposed by [65] based on the NFW profile [66], to describe the small-scale mass distribution of halos and galaxies:

$$\rho(x) = \frac{\rho_0}{x^\gamma \left[1 + x^\alpha\right]^{[\beta-\gamma]/\alpha}}, \tag{2.1}$$



JCAP10(2025)051

where $x = \frac{r}{R_s}$ is a unitless scaled radius from the center and $\rho_0$ is the central pressure, used as a normalization factor. The parameters $\gamma, \alpha, \beta$ are responsible for setting the shape of the slope at inner, intermediate, and outer radii, respectively, where the values for a default NFW profile are $\gamma = 1, \alpha = 1, \beta = 3$.

Halo models utilize a pressure profile, constructed from theory or simulations, to simulate the Compton-$y$ signal. For this study, both the real space and Fourier space predictions utilized the analytic model are detailed in [67], which describes the electron pressure of a galaxy's CGM as a function of mass $M_h$, redshift $z$, and scaled distance to its center $x$:

$$P_e(x; z, M_h) = X_e \frac{\Omega_b}{\Omega_m} P_{200,c}(z, M_h) P_0 \left[\frac{x}{x_c}\right]^{\gamma} \left[1 + \left[\frac{x}{x_c}\right]^{\alpha}\right]^{-\beta}, \tag{2.2}$$

where for $R_s$ we use $R_{200,c}(z, M_h)$, the radius of a sphere centered around a halo of mass $M_h$ with density 200 times the critical density of the universe at redshift $z$. Along with the typical GNFW parameters $\gamma, \alpha, \beta$ which correspond to their equivalents in (2.1) and $P_0$ which takes the place of $\rho_0$, this model includes the core radius $x_c$. In [67], the parameters $P_0, x_c, \beta$ are given mass and redshift dependence and described by a power law:

$$A(z, M_h) = A_0^x \left[\frac{M_{200,c}(z, M_h)}{10^{14} M_\odot}\right]^{\alpha_m^x} [1 + z]^{\alpha_z^x}. \tag{2.3}$$

Throughout this study we fix these models to follow the parameterization of [58], using values of $\gamma = -0.3, \alpha = 1$, fit mass/redshift constant values of $P_0 = 4.67, \beta = 4.01$, and (2.3) for $x_c$ with $\{A_0, \alpha_m, \alpha_z\}^{x_c} = 0.497, -0.00865, 0$.

The amplitude of this profile is then scaled by a characteristic pressure $P_{200,c}$, defined as:

$$P_{200,c}(z, M_h) = \frac{G M_{200,c}(z, M_h)[200\rho_c(z)]}{2R_{200,c}(z, M_h)} \tag{2.4}$$

where $M_{200,c}$ is the mass of a sphere with 200 times the critical density, and converted to electron pressure by multiplying by the baryon fraction $\Omega_b/\Omega_m$ and electron fraction:

$$X_e = \frac{2(X_H + 1)}{5X_H + 3}, \tag{2.5}$$

with values of $\Omega_b = 0.044, \Omega_m = 0.25, X_H = 0.76$.

### 2.2 Halo occupancy distributions

With identical pressure profiles, the goal of this study is to compare the methods used to model the galaxy sample to obtain an average pressure profile. In [58], their sample is divided into four bins of equal size in stellar mass (which is given in the CMASS data) and assigned weights such that $\sum_i w_i \Delta m_{*,i} = 1$, where $\Delta m_{*,i}$ are the size of the stellar mass bins. This study then used the method described in [68] to obtain halo masses from galaxy stellar masses, and uses those and the weights to take a weighted average of halo mass of the pressure profile.

HODs are used to describe how dark matter halos are populated with central galaxies, which reside at the center of their host halos, and satellite galaxies, which orbit around the centrals within the halo. The functional form of an HOD describes the average number of



JCAP10(2025)051

central and satellite galaxies as a function of host halo mass, usually prescribed to have a maximum of one central galaxy and to start adding satellites only after a halo is more like to host a central than not [60]. This framework is modified for each survey to account for the dependence on stellar mass, redshift, and survey incompleteness, resulting in a number of HOD parameterizations between datasets and analyses.

We use the HOD description from [69], which follows the CMASS tailored HOD model in [55], using best-fit parameters they obtained by fitting their halo model against the angular auto-spectra of CMASS galaxies in BOSS DR12 [70] and cross-spectra of *Planck* lensing and tSZ maps [71, 72]. They used a galaxy sample in $0.47 < z < 0.59$ with a median value of $z = 0.53$, splitting there parameterizations into four subsamples distinguished by minimum stellar mass, obtained using the Portsmouth stellar population synthesis code [73]. To most closely match the sample of galaxies in [58], throughout this study we use their parameter values from the subsample of galaxies with $\log M_*/M_\odot > 11.1$ ($N = 473,596$), only varying these values in the analysis in 3.2.

From [69], The average number of centrals in a halo of mass $M_h$ is given by

$$\overline{N_{\rm c}}(M_h) = \frac{f_{\rm inc}(M_h)}{2}\left[1 + {\rm erf}\Big[\frac{\log M_h - \log M_{\rm min}}{\sigma_{\log M_h}}\Big]\right], \tag{2.6}$$

where erf is the error function, $\sigma_{\log M_h} = 0.76$ controls the width or steepness of the transition between none and one central galaxy, and $M_{\rm min} = 13.47$ defines the mass at which halos in the sample are more likely to have a central galaxy than not (as $\overline{N_{\rm c}}(M_h \geq M_{\rm min}) \geq \frac{f_{\rm inc}}{2}$). $f_{\rm inc}(M_h)$ is the incompleteness fraction of the galaxy survey, which is a value between 0 and 1 given by

$$f_{\rm inc}(M_h) = \max\left(0, \min\left(1, 1 + \alpha_{\rm inc}[\log M_h - \log M_{\rm inc}]\right)\right), \tag{2.7}$$

where $\alpha_{\rm inc} = 0.51, M_{\rm inc} = 13.39$ are parameters used in to quantify the incompleteness in CMASS studies [55, 69].

The mean number of satellite galaxies for a given halo mass $M_h$ is given by

$$\overline{N_{\rm s}}(M_h) = \overline{N_{\rm c}}(M_h)\left[\frac{M_h - M_0}{M_1}\right]^{\alpha_s} \mathbb{H}(M_h > M_0), \tag{2.8}$$

where $\mathbb{H}$ is the heaviside function, $\log M_1 = 14.119$ controls the number of satellites galaxies in massive halos, $M_0$ sets the minimum mass required for halos to contain satellite galaxies, and $\alpha_s$ is the index of the power law that defines the satellite galaxy number. Ref. [69] follows previous other studies using a fixed $\alpha_s = 1$ [55, 60]; additionally, they set $M_0 = M_{\rm min}$, effectively stating that halos can start containing satellite galaxies at the same point as centrals.

The radial distribution of satellite galaxies around the halo center $u_s(x)$ is described by the GNFW profile in eq. (2.1) with values of $\alpha = \gamma = 1$ and $\beta_s = 4.38$.

### 2.3 HOD averaged profiles

To probe the pressure profiles of a given galaxy sample, we calculate the galaxy Compton-$y$ cross-power spectrum $P_{gy}(k)$, which can be written as the sum of a one-halo and two-halo component:

$$P_{gy}(k) = P_{gy}^{1h}(k) + P_{gy}^{2h}(k)\,, \tag{2.9}$$



JCAP10(2025)051

where the one-halo component $P_{gy}^{1h}(k)$ comes from the correlation of galaxies and the pressure of their host halo, therefore dominating on scales of the halo radius and smaller, comes from the contribution of galaxies in other halos and overtakes the rapidly decreasing one-halo component on larger scales. These terms are calculated separately in the halo model following the method in [54], with the one-halo term is:

$$P_{gy}^{1h}(k) = \iint y(k;z,M_h)\mathcal{H}(k;z,M_h)n_h(z,M_h)dM_h dz\,, \tag{2.10}$$

where $n_h(z,M_h)$ is the halo mass fraction, the number density of halos with mass $M_h$ at redshift $z$, and $y(k;z,M_h)$ is the Compton-$y$ profile in Fourier space:

$$y(k;z,M_h) = \frac{\sigma_T}{m_e c^2}\frac{4\pi R_{200,c}^3(z,M_h)[1+z]^2}{H(z)}P_e(k;z,M_h)\,, \tag{2.11}$$

where $H(z)$ is the Hubble function, and $P_e(k;z,M_h)$ is the electron pressure profile defined in eq. (2.2) in Fourier space.

$\mathcal{H}(k;z,M_h)$ is the HOD modeled survey fraction of galaxies (both central and satellite) in halos with mass $M_h$ at redshift $z$, defined as:

$$\mathcal{H}(k;z,M_h) = \frac{1}{n_g(z)}\Big[u_c(k;z,M_h)\overline{N_c}(M_h) + u_s(k;z,M_h)\overline{N_s}(M_h)\Big]\,, \tag{2.12}$$

where $\overline{N_c}$ and $\overline{N_s}$ are defined in the previous section, and $n_g(z)$ is the total galaxy number density calculated as:

$$n_g(z) = \int \left[[\overline{N_c}(M_h) + \overline{N_s}(M_h)]\; n_h(z,M_h)\right]dM_h\,, \tag{2.13}$$

and $u_c(k;z,M_h)$ and $u_s(k;z,M_h)$ are the Fourier transformed density profiles for central and satellite galaxies, included to describe the distribution of galaxies within halos. In real space, $u_c$ is set to a Dirac delta at $x=0$ (which transform to $u_c(k;z,M_h)=1$ in harmonic space), equivalent to placing all centrals at the center of halos. Meanwhile, satellite galaxies are distributed around the center of their halos following a GNFW profile described in eq. (2.1) with $\beta$ being a parameter of the HOD model.

The survey-averaged thermal pressure profile can be obtained by taking a weighted integral over the halo mass and redshift range of the survey in harmonic space:

$$\overline{P_{\rm th}^{1h}}(k) = \frac{\iint P_{\rm th}(k;z,M_h)\mathcal{H}(k;z,M_h)n_h(z,M_h)dM_h dz}{\iint \mathcal{H}(k;z,M_h)n_h(z,M_h)dM_h dz}, \tag{2.14}$$

where the combined term $\mathcal{H}(k;z,M_h)n_h(z,M_h)$ acts as a galaxy weight modeling the distribution of the survey.

It follows then that we can calculate the average $y$ profile in the same manner as eq. (2.14) from the one-halo cross-spectra:

$$\overline{y^{1h}}(k) = \frac{P_{gy}^{1h}(k)}{\iint \mathcal{H}(k;z,M_h)\; n_h(z,M_h)dM_h dz} \tag{2.15}$$



JCAP10(2025)051

and obtain an average thermal pressure by performing the inverse conversion of eq. (2.11):

$$\overline{P_{\rm th}^{1h}}(k) = \left[\frac{\sigma_T}{m_e c^2}\frac{\overline{4\pi R_{200,c}^3(z,M_h)[1+z]^2}}{H(z)}\right]^{-1}\overline{y^{1h}}(k) \tag{2.16}$$

where we use mass/redshift averaged values of the prefactor term, calculated in the same method of eq. (2.15), to not reintroduce mass or redshift dependence into the averaged profile. By then taking an inverse Fourier transform, we obtain the one-halo radial profile directly comparable to the results of a non-HOD real space model:

We then construct the total profile through a real space equivalent of eq. (2.9) by adding a two-halo component calculated following [58]:

$$\overline{P_{\rm th}}(r) = \overline{P_{\rm th}^{1h}}(r) + A_{2h} * \overline{P_{\rm th}^{2h}}(r)\,. \tag{2.17}$$

where $\overline{P_{\rm th}^{2h}}(r)$ is the average, over halo mass and redshift, of the two-halo component and $A_{2h}$ is an amplitude term we set to $A_{2h} = 1$. Prior to averaging, The two-halo component is obtained from the inverse Fourier Transform of the two-halo cross-spectra calculated from linear theory following [46]:

$$P_{gy}^{2h}(k;z,M_h) = P_{\rm lin}(k;z)b_h(M_h)\iint y(k;z,M_h)b_h(z,M_h)n_h(z,M_h)dM_h dz \tag{2.18}$$

where $P_{\rm lin}(k)$ is the linear power spectrum and $b_h(M_h)$ is the linear halo bias, and the Compton $y$ profile $y(k;z,M_h)$ is calculated from the GNFW parameterization outlined in [74].

By using the same average two-halo profile from [58], we effectively isolate the analysis of our study to only examine the affects of survey modeling on the one-halo component. This choice is to keep consistency between methodologies: the manners in which our halo model and that of [58]'s calculate the two-halo term are significantly different, containing different implementations for Fourier transforms, halo mass functions, halo biases, integration limits, and modification terms on eq. (2.18), and separating the effects from the addition of an HOD with the rest of the change introduce by two-halo modeling would be difficult. This is permissible as we are not refitting the data in this study, but future forward models will recalculate this component more thoroughly and be able to comment further on possible changes in the results.

### 2.4 Halo model implementation

We used the halo model code `hmvec`[1] to perform the calculations of required cosmological quantities (such as $H(z), n_h(z,M_h), R_{200,c}(z,M_h)$), where we used cosmological values of $h = 0.673, \Omega_m = 0.314 = 1-\Omega_\Lambda, \Omega_b = 0.0491$. `hmvec` is also used to integrate over halo mass and redshift ranges to obtain $P_{gy}^{1h}(k)$, using the composite trapezoidal integration function `numpy.trapz`, and to perform the necessary Fourier transforms to obtain $P_e(k;z,M_h), u_s(k;z,M_h)$, using the one-dimensional discrete fast Fourier transform function `numpy.fft.rfft`, which is implemented as follows:

$$P_e(k_t;z,M_h) = -\frac{\Delta_x}{k_t}\sum_{x=0}^{N_x-1}P_e(x;z,M_h)xe^{\frac{-2\pi i x k_t}{N_x}}, \tag{2.19}$$

[1] https://github.com/simonsobs/hmvec.



JCAP10(2025)051

where $\Delta_x = \frac{x_{\rm max}-x_{\rm min}}{N_x} = \frac{x_{\rm max}-x_{\rm max}/N_x}{N_x}$, and $N_x$ and $x_{\rm max}$ are defined as an input of the halo model. The resulting $P_e(k_t; z, M_h)$ arrays map from wavenumbers $k_t$ provided by the FFT function which correspond to the input $x$ values, a scaled radius measure. The halo model then reassigns the profile arrays to the unscaled wavenumber $k = k_t/R_{200,c}(z, M_h)/[1+z]$, and then interpolates the profile onto an input $k$ array set by the halo model. To transform back into real space, we used the inverse function `numpy.fft.irfft`, and a survey-averaged $\overline{k_t}$ is calculated through the same weighted integral in eq. (2.14), to once again avoid reintroducing mass and redshift dependencies.

As we are trying to ensure consistency between input profiles between our two methodologies to isolate the effects from the HOD inclusion, we make various edits to our halo model to match that of [58]. Both [58] and `hmvec` use the general form of the profiles detailed eqs. (2.1) and (2.2), but there are distinct differences in the usage of mass and redshift values. As opposed to the virial halo mass $M_{\rm vir}$ in [58], our halo model uses a mass definition of $M_{200c}$, which it uses to calculate the profiles $\rho(x)$ and $P_e(x; z, M_h)$, as well as the parameter within them, such as $R_{200,c}$ (and therefore $x$), $P_{200,c}$, $P_0$, $x_c$, and $\beta$. For this analyses, we edited our halo model to use the virial halo mass. Furthermore, in [58] the $P_{200,c}$ and $\beta$ values in the pressure profile were fixed, while the parameter $x_c(z, M_h)$ is determined from the mean redshift and halo mass, leaving only $R_{200,c}$ to change over the integration. This is different than our halo model, which varies all parameters through mass and redshift, and therefore finds an average pressure profile instead of the pressure profile at average values. To ensure that these misalignments are not creating artificial differences in our final results, we customized our halo model to match the mass and redshift values and treatment of parameters as in [58], and therefore ensure that the matter and pressure profiles being used for both methods were identical. Additionally, Our halo model adds a window function to the one-halo term in the pressure profile by applying a window function before performing the transform in eq. (2.19), resulting in the one-halo contribution to be zero at regions beyond $R_{\rm vir}/R_{200,c}$; as it is not performed in [58], we remove this step in our halo model. Furthermore, we restricted the mass range of our halo model to only cover the CMASS bins used in [58], $12.12 < \log_{10}(M_h/M_\odot) < 13.98$.

We further checked our calculations in sections 2.1–2.3 against another halo model `class_sz`[2] [75], finding consistent values for the galaxy-$y$ cross-spectra when using the same profiles in (2.2) and the same HOD parameterization in eqs. (2.6) and (2.8).

### 2.5 Projected tSZ signal

In [58], the authors projected the modeled profiles onto the sky to forecast direct observations of the tSZ signal stacked on galaxies. Following their methods, we use the `mop-c-gt`[3] as implemented in `SOLikeT`,[4] a likelihood package designed for use with the Simons Observatory. The projected average thermal pressure profile is calculated by integrating over the line of sight distance $l$:

$$\overline{P_{\rm th}}^{2D}(R) = 2\int_0^\infty \overline{P_{\rm th}}\Big(r = \sqrt{l^2 + R^2}\Big) dl\,, \tag{2.20}$$

[2] https://github.com/CLASS-SZ.
[3] https://github.com/samodeo/Mop-c-GT.
[4] https://github.com/simonsobs/SOLikeT.



JCAP10(2025)051

where $R(\theta) = \theta d_A(\bar{z})$ is the projected size of the sky using a survey-averaged redshift. As detailed in [59], the array of $l$ values should be fine enough and cover a large enough range to account for the entire profile in detail; too large a $l_{\rm min}$ or too small a $l_{\rm max}$ prohibitively restricts the $r$ range. We find that extending the integration range beyond $l = 10^{-4} - 50$ Mpc or using more than 50 logarithmically spaced bins has a negligible effect on the results, and therefore is sufficient to capture the entire signal

Additionally, as this and following integrals will cover values of $r(R, l)$ that are below the lowest value of $r$ returned by the halo model, we take advantage of the plateau that occurs in the pressure profile at about $10^{-3}$ Mpc to extrapolate that value of $\overline{P_{\rm th}}(r)$ for any $r$ values outside the normal range.

Combining this with eqs. (1.1) and (1.2), the final modeled tSZ signal is:

$$\Delta T_{\rm tSZ}(\theta; \nu) = T_{\rm CMB}\ f(\nu)\ \frac{\sigma_T X_e}{m_e c^2}\ \overline{P_{\rm th}}^{2D}(\theta)\,. \tag{2.21}$$

To account for the effects of the instrument, the signal is convolved with the beam of the instrument and is filtered using aperture photometry:

$$\tilde{T}_{tSZ}(\theta_d) = \int [T_{tSZ}(\theta)\ \circledast\ B(\theta)]\ W_{\theta_d}(\theta)\ d^2\theta\,, \tag{2.22}$$

where $B(\theta)$ is the instrument beam convolved using a Hankel transform described in [59], $\theta_d$ is the aperture radius, and

$$W_{\theta_d}(\theta) = \begin{cases} 1 & \theta < \theta_d\,, \\ -1 & \theta_d \le \theta \le \sqrt{2}\theta_d\,, \\ 0 & \theta_d > \sqrt{2}\theta_d\,. \end{cases} \tag{2.23}$$

### 2.6 Miscentering

In a typical halo model, central galaxies are placed directly in the center of a halo, and therefore aligned with the pressure profile of that halo, while satellite galaxies are equally distributed at a distance from the halo center. This is based off the assumption that halo centers are properly identified and aligned with the galaxies within them; however, if a considerable portion of galaxies are misaligned within the pressure profile of their host halo, this would dampen the cross-correlation signal. In the mass-averaged pressure profiles, this would manifest as a decrease in the signal at lower scales, with a boost at some scale corresponding to description of the miscentered galaxies. Miscentering of clusters has been shown to be capable of producing significant offsets in SZ measurements, which could explain discrepancies between observations and models [76]. To incorporate this effect into our analysis, we follow the formalism used in [62] which follows [77] to model miscentered galaxies in calculating the lensing signal from clusters, replaced the lensing signal $\Delta\Sigma$ with the projected average thermal pressure detailed in eq. (2.20):

$$\overline{P_{\rm th,\ mis}}^{2D}(R) = [1 - f_{\rm mis}]\overline{P_{\rm th}}^{2D}(R) + f_{\rm mis}\overline{P_{\rm th,\ mis}}^{2D}(R)\,, \tag{2.24}$$

where $f_{\rm mis}$ is the fraction of miscentered galaxies and $\overline{P_{\rm th,\ mis}}^{2D}(R)$ is the averaged profile for miscentered galaxies, obtained by taking a weighted integral over the range of possible



JCAP10(2025)051

miscentering values:

$$\overline{P_{\rm th,\ mis}}^{2D}(R) = \int \overline{P_{\rm th,\ mis}}^{2D}(R|R_{\rm mis})\ p(R_{\rm mis})\ dR_{\rm mis}\,, \tag{2.25}$$

where we integrate over $R_{\rm mis} = 2 \times 10^{-4} - 20$ Mpc with 100 logarithmically spaced bins, $\overline{P_{\rm th,\ mis}}^{2D}(R|R_{\rm mis})$ is the profile for a miscentering value of $R_{\rm mis}$, obtained by taking the azimuthal average of the surface thermal pressure:

$$\overline{P_{\rm th,\ mis}}^{2D}(R|R_{\rm mis}) = \frac{1}{2\pi}\int_0^{2\pi} \overline{P_{\rm th}}^{2D}\Big(R'(R, R_{\rm mis}, \theta)\Big)d\theta\,, \tag{2.26}$$

where $R'(R, R_{\rm mis}, \theta) = \sqrt{R^2 + R_{\rm mis}^2 + 2RR_{\rm mis}\cos\theta}$ using 50 linearly spaced bins, and $p(R_{\rm mis})$ is the distribution of miscentering values of the model, which we set as a Gamma distribution following [62]:

$$p(R_{\rm mis};\tau) = \frac{R_{\rm mis}}{[\tau R_h]^2}\exp\left(-\frac{R_{\rm mis}}{\tau R_h}\right), \tag{2.27}$$

where $\tau = R_{\rm mis}/R_h$ is a dimensionless miscentering offset that sets the peak of the distribution, and we set the halo radius $R_h = \overline{R_{200,c}}$.

## 3 Results

We find that after several corrections and consistency edits, the two methods of generating theoretical predictions for the tSZ signal produce results similar in shape but noticeably different in scale. As shown in figure 1, Our model generates a signal stronger than that from [58] by about $\sim 20\% - 25\%$, depending on the radius, improving the $\chi^2$/DOF by 33%. While there exists some level of uncertainty as a result of small differences between the samples used in the two studies, this is a larger deviation than would be expected and displays the marked improvement of our more detailed methodology over the one used in [57, 58, 78]. After accounting for different ways of modeling the mass distribution of the CMASS sample, it is the inclusion of satellites that has the largest impact on this tSZ signal because satellite galaxies populate more massive central galaxy/group with larger tSZ signals. The previous models would use the mass of the satellite for the tSZ signal, where instead it should be the satellite and its central galaxy/group. Here, the galaxy/group will dominate the signal given the steep mass scaling of $M^{5/3}$ of the tSZ signal, so at percent level accuracy the satellite contribution is negligible. This is explored more in the following subsections.

### 3.1 Implementation effects

As shown in figure 2, there are several choices that we have to make in the halo model implementation which can wind up having moderate to significant effects on the final signal.

Even after ensuring the same thermal pressure profile for any given value of $r$, $z$, and $M_h$, there is still a significant dependence on the properties of the halo masses being used for averaging. Primarily, this is seen in the halo mass integration range: increasing the maximum halo mass includes more large halos with stronger pressure profiles, raising the average halo mass and therefore strengthening the pressure profile overall [59]. As shown in figure 2, even



JCAP10(2025)051

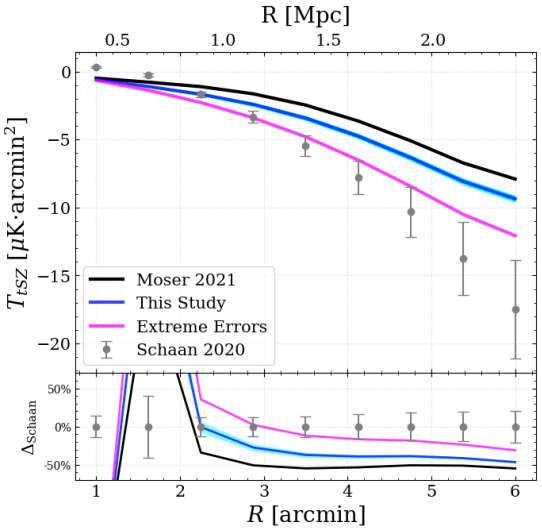


**Figure 1.** Modeled observable tSZ signal from our HOD study (blue), with a $1\sigma$ confidence interval from the HOD parameter uncertainties, and from the methodology of [58] (black), both containing an estimated dust profile from [57], compared to the ACT DR5 data results from [50] (grey), with % deviations from the data shown below. While our study is unable to resolve the discrepancy between predicted and observed signals, the new modeling process yields a result that is more similar to the data than older results. Constructing a "worst case" scenario by selectively combining the offset sources discussed in this paper to maximize the predicted signal results in a closer match to data at larger angular scales at the expense of creating larger gaps at lower scales (magenta).

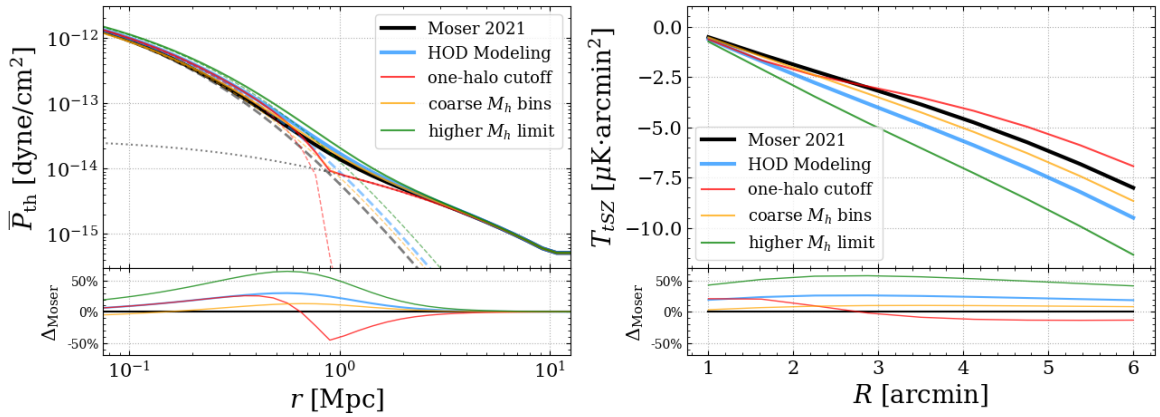


**Figure 2.** Modeled survey-averaged thermal pressure profile (left) and corresponding projected tSZ signal (right) using the methodology from [58] (black) and the HOD modeling of this study (blue), with % differences from [58] shown below. Additionally shown are the results when incorrectly including inconsistencies such as a cutoff radius to the one halo term (red), very coarse bins for halo mass (yellow), and a higher upper limit of halo mass range (green), all of which cause significant deviations. Dashed and dotted lines represent the one-halo and two-halo component, respectively, where the latter is held constant throughout this study.

JCAP10(2025)051

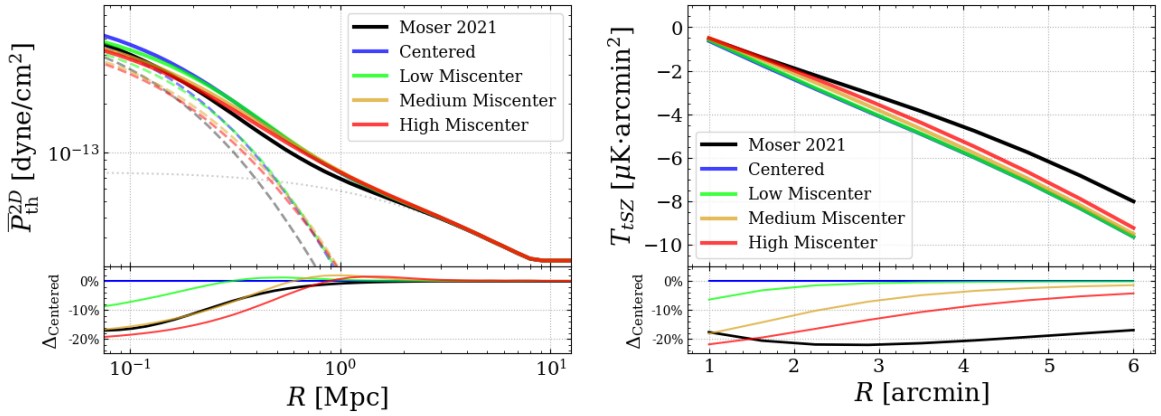


**Figure 3.** Projected modeled survey-averaged thermal pressure profiles (left) and corresponding observable tSZ signal (right) from [58] (black), using our HOD modeling without miscentered central galaxies (blue), and with 25% of central galaxies miscentered at low (green), moderate (yellow), and high (red) radii, $R_{\rm mis} = 0.1, 0.3, 0.5$ Mpc respectively, with % deviations from the centered model shown below. Miscentering is shown to dampen the signal more strongly for higher values of miscentering distance and at lower angular scales. Also included is the results from [58] (black).

a 50% higher $M_h$ upper limit on the integration increases the difference from 20% to 50%. Additionally, changing these mass ranges affects the fraction of central/satellite galaxies within the survey, which are entirely dependent on the halo mass as shown in eq. (2.6) and (2.8), which alters the shape of the profile. This sensitivity makes it crucially important to use halo bounds that are informed by the galaxy distributions of the sample being modeled, to avoid integrating over ranges where the sample has negligible halo counts. Another effect is the choice of binning, both in number and spacing. Even with both models using logarithmically spaced bins, we found that changing our bin number by less than an order of magnitude can affect the signal by $10 - 20\%$, and therefore used the same value in both methodologies to keep consistencies. The bin number we selected was determined by finding the value at which increasing the fineness no longer discernibly changes the final signal in order to properly collect contribution from halos of all masses in the sample; a process that should be repeated in future studies, as the ideal bin number could change across galaxy distributions.

The combination of a GNFW one-halo term and a two-halo profile measurably improves the quality of the model, as shown in [58], but introduce the risk of double-counting pressure due to halo exclusion effects, which arise from describing halos as non-overlapping objects. Furthermore, studies have shown that the halo profiles drop off more steeply than a GNFW at their outer radius [79], motivating some studies to introduce smoothing factors and/or cutoff to better model the transition region [56, 57]. This cutoff procedure significantly changes the shape and scale of the average pressure profile, as can be seen in the dashed red line in figure 2.

While it would be misguided to uncritically use miscentering values from redMaPPer to model CMASS galaxies, we use these results to estimate the effects of miscentering on our signal. Ref. [80] showed that redMaPPer clusters have a miscentering fraction of about $f_{\rm mis} = 25\%$ and a miscentering offset value of about $\tau = 0.17$, which translates to a miscentering distance of about $0.15 \lesssim R_{\rm mis} \lesssim 0.2$ (using their radius definition $R_\gamma$

JCAP10(2025)051

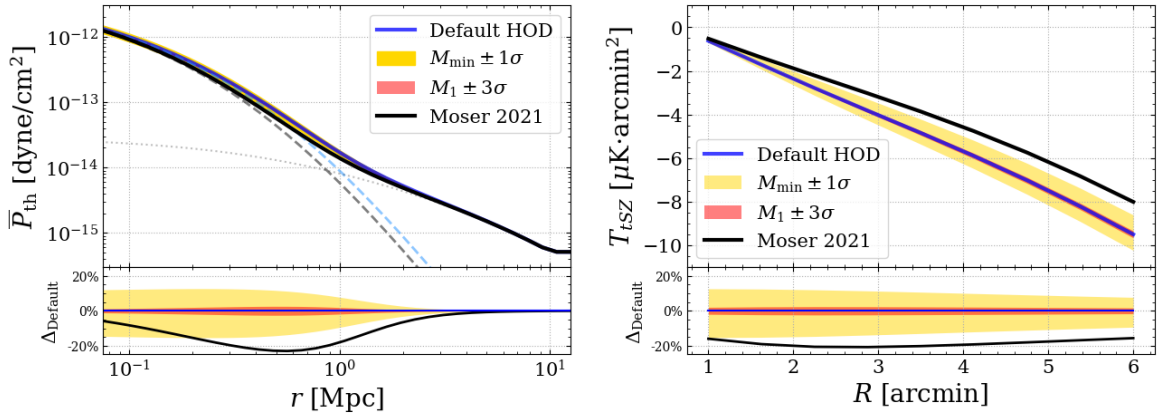


**Figure 4.** Modeled survey-averaged thermal pressure profiles (left) and corresponding observable tSZ signal (right) from the methodology of [58] (black), using our HOD modeling with the default HOD parameters (blue), and showing regions of error resulting from $1\sigma$ deviations in the HOD parameter $M_{\rm min}$ (yellow) and $3\sigma$ deviations in the HOD parameter $M_1$ (red), with % deviations to default results shown below. While changes in $M_{\rm min}$ have a clear effect, even unreasonably large changes in $M_1$ barely move the results as a result of nearly all satellite galaxies being cut off by the mass range of the halo model.

based off cluster richness $\gamma$); we use the same miscentering fraction $f_{\rm mis}$ and select three miscentering distances $R_{\rm mis} = \tau R_h = 0.1, 0.3, 0.5$ Mpc to examine the effects at different quantities. As shown in figure 3, our model acts as expected, weakening the pressure at low $R$ and strengthening it at high $R$, with higher $R_{\rm mis}$ or $f_{\rm mis}$ values both increasing the degree of the effect; however, after transforming this to a final $T_{\rm tSZ}$ signal, we see a weakening effect which is more potent at small scales, but we see no strengthening in the signal at any scale. We attribute this to the aperture filter applied in the transform which removes higher radii. We attempt to set a very low $R_{\rm mis}$ value to keep the profiles within the aperture, and see the increase at higher radii, but with such a small difference this strengthening effect is also very small to the point of negligible. The inclusion of satellites in the tSZ modeling is similar to that of miscentering, since the halo center will be that of the satellite which is off-centered from the peak on the pressure profile which is centered on the halo. In a way these two effects are degenerate with one another.

### 3.2 HOD parameters

Within the HOD model the different parameters have different physical meanings and influences on the final results. We discuss the impact of the different parameters below.

$\log M_{\rm min}$ (occasionally denoted as $\log M_{\rm cut}$) is the most influential parameter in our HOD (partially a results of setting $M_0 = M_{\rm min}$), as changing this parameter effectively changes the galaxies being selected: a very high value selects only galaxies with more massive halos, and a small value allows less massive halos (and hence less massive central galaxies) into the analysis. As a result, the value of this parameter has a strong effect on the average pressure profile, as the inclusion of less or more massive galaxies will yield a stronger or weaker pressure profile, respectively, just from the density and concentration of matter. It should be noted that this effect will also be dependent on the mass range being imposed



JCAP10(2025)051

on the analysis, as changing $M_{\rm min}$ from a value of $10^{13}M_\odot$ to $10^{12}M_\odot$ will be less prevalent if only averaging starting with halos at $M_h \geq 10^{12.95}M_\odot$ to match your survey. It would increase the number of galaxies in low mass halos towards the bounds, but would include no new galaxies in halos below the minimum mass in the actual average.

$\sigma_{\log M}$ (occasionally denoted as $\sigma/\sigma_M/\sqrt{2}\sigma$) also is influential in $N_c$, and decreasing/increasing this parameter yields a steeper/smoother transition from 0 to 1 at $M_{\rm min}$. Then, lowering the value of $\sigma_{\log M}$ spreads some of the halo mass right above the minimum mass to right below the minimum mass, effectively including more low masses and less higher masses, which has the effect of weakening the pressure profile. This parameter is therefore highly degenerate with $M_{\rm min}$ (though the profile is not as sensitive to changes in $\sigma_{\log M}$) and as a result, changing both parameters allows changing the shape of the mean number distribution while keeping the same mean mass in the analysis. Variations $\alpha_{inc}$ and $M_{inc}$, which are used to calculate $f_{inc}$, cause small changes in the amplitude of the pressure profile without changes to the shape.

$\log M_1$ controls the number of satellite galaxies, and increasing this value raises the benchmark for satellite to exist in halos and therefore filters out galaxies in high mass halos, lowering the pressure profile. However, in our analysis, the value of $\log M_{\rm min}$ is very close to the highest possible mass defined by our bins. While the $\sigma_m$ parameter in the $N_c$ term allows for some spread and therefore halos to exist below this value, in the $N_s$ equation this is a hard cutoff, and therefore practically zeroes the number of satellite galaxies in this survey regardless of $\log M_1$. This is shown in figure 4, where we see that $3\sigma$ error values on $M_1$ still have very little effect on the tSZ signal, and are dwarfed by the effect of $\log M_{\rm min}$. To examine the effect of this parameter, we therefore had to artificially lower the value of $\log M_{\rm min}$ into the range set by the mass bins. We also explored changes in the value of $\beta_s$, but found that changing this parameter had no noticeable effect on the pressure profiles, even with $\log M_{\rm min}$ shifted to artificially include more satellites.

## 4 Discussions and conclusions

We find that differences in survey modeling methodology does manifest in significant differences in predicted tSZ signals. As shown in figure 1, our study using HOD modeled profiles produces a better fit to the data, improving the $\chi^2$/DOF by 33%, from 3.88 to 2.60, and the probability to exceed value by 3576%, from $3.1\times10^{-4}$ to 0.011. This is mainly a result of the HOD methodology producing a $\sim 25\%$ stronger tSZ signal than the methodology in [58], which we attribute partially to a more accurate modeling of satellite galaxies. This brings the modeled signal, which severely under predicts measurements, closer to the data on angular scales above 2' (we exclude scales below this in our as they are affected by heavy dust contamination, beyond the scope of this paper). It should be noted that this is a significant result, as we find using the HOD parameterizations from different surveys in our forward model produces similar differences in signal as shown in figure 5, suggesting that inconsistencies between studies on their survey modeling can be as consequential as modeling an entirely separate sample of galaxies.

Individual variations with a $1\sigma$ range of in the HOD parameters, which manifest as alterations in the fraction of satellite galaxies, could account for $10-20\%$ variations in the tSZ signal, but altogether the errors obtained from using the output of chains from the



JCAP10(2025)051

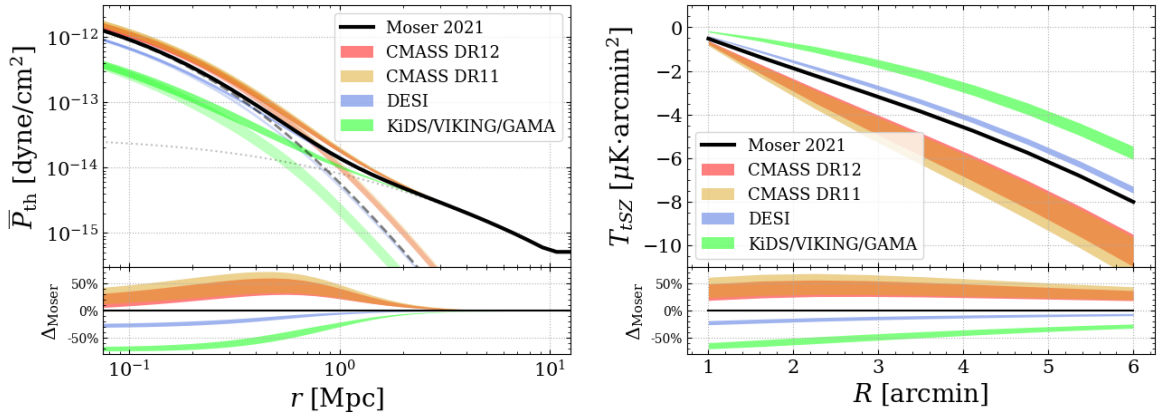


**Figure 5.** Average thermal pressure profiles and projected tSZ signal for several different HOD parameterizations, shown in bands to indicate the range of profiles for the subsets detailed in the studies, divided by stellar mass or redshift. Ref. [69] (red) and [55] (yellow) both model the CMASS galaxy sample examined in this study, while HODs for DESI LRGs [81] (blue) and KiDSxVIKING/GAMA [82] (green) are included to show the larger difference between HOD models of different galaxy samples. The non-HOD model results [58] show similar levels of deviation from HOD model results its modeled survey (CMASS) as completely different surveys, showing the significance of the modeling methodology on final profile results.

HOD parameter fitting process show tight constraints on the signal. Furthermore, there are unique systematics introduced with each method that will need to be accounted for on when comparing different studies and datasets. We also examine the effect of miscentering on observed tSZ signals finding that it is capable of dampening the signal by equivalent amounts at low angular sizes.

We explore the results if several of the effects in this paper are combined, specifically a 50% higher halo mass limit, a $+1\sigma$ error on $M_{\rm min}$, and a $R_{\rm mis} = 0.5$ miscentering on 25% of central galaxies. In this case, our predicted signal aligns much more closely with the data at larger angular scales, at the expense of increasing the gap at smaller angular scales. While it is unreasonable to believe that modeling errors would both be this extreme and all point in the direction of a stronger signal, this shows that there is weight to the idea that the disagreements between data and models are the result of several separate, smaller effects, and therefore continued refining of each step in the analysis pipeline is essential going forward.

This study focused specifically on the implementation effects of forward modeling profiles to predicted measurements on the final signal, there are various other components in the full pipeline that have significant influence on the results. While we used a fixed model of thermal pressure, changes in the parametrization or deviation from a GNFW form for the one-halo term can account for unaligned theory and measurement and shown in [57] where the authors use free parameters in the profile model to fit their measurements. Similarly, the two-halo term is described in such studies with a fit amplitude parameter and an unchanging profile constructed which is known to be unreliable; more detailed modeling of this term with the addition of mass/redshift dependence could show substantial differences in our predictions. There are also possible complications within the measurement itself, especially



JCAP10(2025)051

| Effect | $T_{tsz}(R < 2')$ | $T_{tsz}(R > 3')$ | $\Delta\%_{\rm sat}$ |
|---|---|---|---|
| 5 $M_h$ bins | -15% | -10% | -1.7% |
| +50% max $M_h$ | +22% | +22% | +2.1% |
| -50% min $M_h$ | -2% | -1% | 0% |
| one-halo cutoff | -1% | -28% | N/A |
| | | | |
| $\log M_{\rm min} \pm 1\sigma$ | $\pm$13% | $\pm$9% | $\mp$1% |
| $\log M_1 \pm 1\sigma$ | $\pm$0.7% | $\pm$0.6% | $\pm$0.5% |
| | | | |
| Low Miscent. | -5% | 0% | N/A |
| Med. Miscent. | -15% | -5% | N/A |
| High Miscent. | -20% | -10% | N/A |

**Table 1.** Table of various implementation choices in our HOD forward modeling procedure discussed in this paper and their effect on the final tSZ signal, shown as % differences from the final modeled signal of our study at small and large angular scales. Also shown is the changes in the percent of satellite galaxies in the modeled survey $\%_{\rm sat}$ from the default value of 4.3%.

concerning dust and the Cosmic Infrared Background (CIB), which is difficult to properly account for and has a profound impact on the signal at smaller radii; the author in [57] outlined a procedure for fitting dust profiles using large-sky dust maps, and improved CIB modeling and upcoming data could move future measurement more in line with our models.

Recently, work by [83] looked at the impact of satellites on the kSZ cross-correlation measurements [84] using numerical simulations. They found that including all satellite halos down to a given stellar mass threshold changed their predicted kSZ signal for CMASS galaxies up to 30%. Similar to the tSZ result shown in this work, these kSZ changes are the result of satellite galaxies residing in more massive dark halos hence larger SZ signals. Interestingly the change induced by the inclusion of satellites in kSZ signal that [83] found has a similar amplitude to what we found for tSZ signal. However, with simple mass scaling arguments for the kSZ ($\propto M$) and the tSZ ($\propto M^{5/3}$), one would expect that impact on the tSZ signal should be larger than the kSZ signal. One essential, difference between these two analyses is that our HOD implementation models the selection of CMASS galaxies through the $M_0$ and $M_1$ parameters which account for the fact that CMASS galaxies were selected to be predominantly central galaxies and have a small satellite fraction for their stellar mass threshold according to clustering and weak-lensing measurements [69, 85–87]. Hence, the impact that the inclusion of satellites has on the tSZ signal in our methodology is not as large as if we were to include all galaxies (central and satellites) above a threshold mass disregarding how the CMASS galaxies were selected.

As upcoming observations continue to increase in scope and fidelity, the need for improved theoretical model of these future signals is made clear by this work. Next generation CMB experiments like the Simons Observatory [88] and CMB-S4 [89] will provide high fidelity



JCAP10(2025)051

and resolution measurements of the tSZ (and kSZ) by improving upon ACT, and current and upcoming galaxy surveys like the Dark Energy Spectroscopic Instrument (DESI) have a target density over ten times that of CMASS [90]. As both will cover a larger fraction of the sky the overlap between the observations will also increase, and as the inherent noise is reduced by a factor of the square root of the number of galaxies in the study, this further improves the signal. Proper usage of HODs in halo models will be critical to quantifying galaxy properties of these future measurements.

We note that while the results should be broadly applicable, and our process is able to use any given HOD as shown in figure 5, some of the analysis done in this project is specific to the HOD fitted for CMASS. Other HODs may include or omit other parameters that are explored in this project. For example, HODs being constructed for the DESI survey do not explore deviation from the standard NFW profile [81, 91–93].

For this study, pressure profiles are obtained using the analytic model described in [67] (shown in section 2.1) as is standard for halo model calculations. We note that the initial pressure profile parameters were fit to simulations clusters with halo mass of $M_{200,c} > 5 \times 10^{13} M_{\odot}$, which is above the mass range of CMASS halos. [57] obtained a parameterization of eq. (2.2) by fitting the measurements in [50], without the use of simulations; going forward such fits should use the forward model with an HOD outlined in this study. Multiple types of profiles can also be obtained through hydrodynamical simulations such as IllustrisTNG [94–98] and SIMBA [99], through stacking simulated galaxies or through emulators [78, 100]. The predictions produced from such studies have similarly yielded a poor fit to observations, and have further shown that the modeled signal can be improved by increasing the strength of feedback in simulations [78, 84]. The addition of the The CAMELS project [101, 102], which has already shown encouraging results and continues to improve in detail and in size, is key for future comparison to simulations, where the parameters of sub-models which control feedback processes are varied.


## Acknowledgments

We are grateful to Simone Ferraro, Emmanuel Schaan, and Sandy Yuan for their helpful feedback and useful discussions. NB acknowledges support from NASA grants 80NSSC18K0695 and 80NSSC22K0410. JCH acknowledges support from NSF grant AST-2108536, NASA grant 80NSSC22K0721 (ATP), the Sloan Foundation, and the Simons Foundation.


## References


[1] M. Fukugita and P.J.E. Peebles, *The cosmic energy inventory*, *Astrophys. J.* **616** (2004) 643 [astro-ph/0406095] [INSPIRE].

[2] A. Gallazzi, J. Brinchmann, S. Charlot and S.D.M. White, *A census of metals and baryons in stars in the local universe*, *Mon. Not. Roy. Astron. Soc.* **383** (2008) 1439 [arXiv:0708.0533] [INSPIRE].

[3] C. Federrath, *Inefficient star formation through turbulence, magnetic fields and feedback*, *Mon. Not. Roy. Astron. Soc.* **450** (2015) 4035 [arXiv:1504.03690].




JCAP10(2025)051

[4] M. Fukugita, C.J. Hogan and P.J.E. Peebles, *The cosmic baryon budget*, *Astrophys. J.* **503** (1998) 518 [astro-ph/9712020] [INSPIRE].

[5] R. Cen and J.P. Ostriker, *Where are the baryons? 2. Feedback effects*, *Astrophys. J.* **650** (2006) 560 [astro-ph/0601008] [INSPIRE].

[6] J.N. Bregman, *The search for the missing baryons at low redshift*, *Ann. Rev. Astron. Astrophys.* **45** (2007) 221 [arXiv:0706.1787] [INSPIRE].

[7] T. Di Matteo, V. Springel and L. Hernquist, *Energy input from quasars regulates the growth and activity of black holes and their host galaxies*, *Nature* **433** (2005) 604 [astro-ph/0502199] [INSPIRE].

[8] V. Springel, T. Di Matteo and L. Hernquist, *Modeling feedback from stars and black holes in galaxy mergers*, *Mon. Not. Roy. Astron. Soc.* **361** (2005) 776 [astro-ph/0411108] [INSPIRE].

[9] C. Scannapieco, P.B. Tissera, S.D.M. White and V. Springel, *Effects of supernova feedback on the formation of galaxy disks*, *Mon. Not. Roy. Astron. Soc.* **389** (2008) 1137 [arXiv:0804.3795] [INSPIRE].

[10] R.S. Somerville et al., *A semi-analytic model for the co-evolution of galaxies, black holes, and active galactic nuclei*, *Mon. Not. Roy. Astron. Soc.* **391** (2008) 481 [arXiv:0808.1227] [INSPIRE].

[11] A. Marasco et al., *The effect of stellar feedback on a Milky Way-like galaxy and its gaseous halo*, *Mon. Not. Roy. Astron. Soc.* **451** (2015) 4223 [arXiv:1506.00652].

[12] R.S. Somerville and R. Davé, *Physical models of galaxy formation in a cosmological framework*, *Ann. Rev. Astron. Astrophys.* **53** (2015) 51 [arXiv:1412.2712] [INSPIRE].

[13] O. Agertz and A.V. Kravtsov, *The impact of stellar feedback on the structure, size, and morphology of galaxies in Milky-Way-sized dark matter halos*, *Astrophys. J.* **824** (2016) 79 [arXiv:1509.00853] [INSPIRE].

[14] J. Tumlinson, M.S. Peeples and J.K. Werk, *The circumgalactic medium*, *Ann. Rev. Astron. Astrophys.* **55** (2017) 389 [arXiv:1709.09180].

[15] C.C. Steidel et al., *The structure and kinematics of the circum-galactic medium from far-UV spectra of $z \sim 2$–3 galaxies*, *Astrophys. J.* **717** (2010) 289 [arXiv:1003.0679] [INSPIRE].

[16] N.M. Nielsen et al., *MAGIICAT V. Orientation of outflows and accretion determine the kinematics and column densities of the circumgalactic medium*, *Astrophys. J.* **812** (2015) 83 [arXiv:1505.07167].

[17] M.S. Peeples et al., *Understanding the circumgalactic medium is critical for understanding galaxy evolution*, arXiv:1903.05644.

[18] K.M. Lanzetta, D.V. Bowen, D. Tytler and J.K. Webb, *The gaseous extent of galaxies and the origin of Lyman-$\alpha$ absorption systems: a survey of galaxies in the fields of Hubble space telescope spectroscopic target QSOs*, *Astrophys. J.* **442** (1995) 538 [INSPIRE].

[19] H.-W. Chen et al., *The gaseous extent of galaxies and the origin of QSO absorption line systems*, in the proceedings of the *10th Rencontres de Blois on the birth of galaxies*, (1998) [astro-ph/9809297] [INSPIRE].

[20] J. Tumlinson et al., *The large, oxygen-rich halos of star-forming galaxies are a major reservoir of galactic metals*, *Science* **334** (2011) 948 [arXiv:1111.3980] [INSPIRE].



JCAP10(2025)051

[21] G.C. Rudie et al., *The gaseous environment of high-z galaxies: precision measurements of neutral hydrogen in the circumgalactic medium of $z \sim 2$–3 galaxies in the Keck baryonic structure survey*, *Astrophys. J.* **750** (2012) 67 [arXiv:1202.6055] [INSPIRE].

[22] J. Tumlinson et al., *The COS-halos survey: rationale, design, and a census of circumgalactic neutral hydrogen*, *Astrophys. J.* **777** (2013) 59 [arXiv:1309.6317] [INSPIRE].

[23] J.K. Werk et al., *The COS-halos survey: physical conditions and baryonic mass in the low-redshift circumgalactic medium*, *Astrophys. J.* **792** (2014) 8 [arXiv:1403.0947] [INSPIRE].

[24] H.-W. Chen et al., *Characterizing circumgalactic gas around massive ellipticals at $z \sim 0.4$ — I. Initial results*, *Mon. Not. Roy. Astron. Soc.* **479** (2018) 2547 [arXiv:1805.07364].

[25] EBOSS collaboration, *The circumgalactic medium of eBOSS emission line galaxies: signatures of galactic outflows in gas distribution and kinematics*, *Astrophys. J.* **866** (2018) <bbl:err:pages> [arXiv:1806.05786] [INSPIRE].

[26] F.S. Zahedy et al., *Characterizing circumgalactic gas around massive ellipticals at $z \sim 0.4$ — II. Physical properties and elemental abundances*, *Mon. Not. Roy. Astron. Soc.* **484** (2018) 2257 [arXiv:1809.05115].

[27] M.C. Wilde et al., *CGM2 I: the extent of the circumgalactic medium traced by neutral hydrogen*, *Astrophys. J.* **912** (2021) 9 [arXiv:2008.08092].

[28] E. Borisova et al., *Ubiquitous giant Ly $\alpha$ nebulae around the brightest quasars at $z \sim 3.5$ revealed with MUSE*, *Astrophys. J.* **831** (2016) 39 [arXiv:1605.01422] [INSPIRE].

[29] B.H.C. Emonts et al., *Molecular gas in the halo fuels the growth of a massive cluster galaxy at high redshift*, *Science* **354** (2016) 1128 [arXiv:1612.00387].

[30] M. Ginolfi et al., *Molecular gas on large circumgalactic scales at $z = 3.47$*, *Mon. Not. Roy. Astron. Soc.* **468** (2017) 3468 [arXiv:1611.07026] [INSPIRE].

[31] L. Wisotzki et al., *Nearly all the sky is covered by Lyman-$\alpha$ emission around high-redshift galaxies*, *Nature* **562** (2018) 229 [arXiv:1810.00843].

[32] F. Arrigoni Battaia et al., *Discovery of intergalactic bridges connecting two faint $z \sim 3$ quasars*, *Astronomy & Astrophysics* **631** (2019) A18 [arXiv:1909.00829].

[33] F. Leclercq et al., *The MUSE Hubble ultra deep field survey: XIII. Spatially resolved spectral properties of Lyman-$\alpha$ haloes around star-forming galaxies at $z > 3$*, *Astronomy & Astrophysics* **635** (2020) A82 [arXiv:2002.05731].

[34] J. Zabl et al., *MusE GAs FLOw and Wind (MEGAFLOW) VIII. Discovery of a MgII emission halo probed by a quasar sightline*, *Mon. Not. Roy. Astron. Soc.* **507** (2021) 4294 [arXiv:2105.14090] [INSPIRE].

[35] B.D. Oppenheimer and R. Dave, *Mass, metal, and energy feedback in cosmological simulations*, *Mon. Not. Roy. Astron. Soc.* **387** (2008) 577 [arXiv:0712.1827] [INSPIRE].

[36] A.B. Ford et al., *Hydrogen and metal line absorption around low-redshift galaxies in cosmological hydrodynamic simulations*, *Mon. Not. Roy. Astron. Soc.* **432** (2013) 89 [arXiv:1206.1859] [INSPIRE].

[37] C.B. Hummels, B.D. Smith and D.W. Silvia, *Trident: a universal tool for generating synthetic absorption spectra from astrophysical simulations*, *Astrophys. J.* **847** (2017) 59 [arXiv:1612.03935].

[38] J. Suresh et al., *On the OVI abundance in the circumgalactic medium of low-redshift galaxies*, *Mon. Not. Roy. Astron. Soc.* **465** (2016) 2966 [arXiv:1511.00687].



JCAP10(2025)051

[39] C.B. Hummels et al., *The impact of enhanced halo resolution on the simulated circumgalactic medium*, *Astrophys. J.* **882** (2019) 156 [arXiv:1811.12410].

[40] BOSS collaboration, *The clustering of galaxies in the completed SDSS-III Baryon Oscillation Spectroscopic Survey: cosmological analysis of the DR12 galaxy sample*, *Mon. Not. Roy. Astron. Soc.* **470** (2017) 2617 [arXiv:1607.03155] [INSPIRE].

[41] ACT collaboration, *The Atacama Cosmology Telescope: DR6 gravitational lensing map and cosmological parameters*, *Astrophys. J.* **962** (2024) 113 [arXiv:2304.05203] [INSPIRE].

[42] Y. Oren et al., *Sunyaev-Zeldovich signals from $L^*$ galaxies: observations, analytics, and simulations*, arXiv:2403.09476.

[43] R.A. Sunyaev and Y.B. Zeldovich, *Small-scale fluctuations of relic radiation*, *Astrophys. Space Sci.* **7** (1970) 3 [INSPIRE].

[44] R.A. Sunyaev and Y.B. Zeldovich, *The observations of relic radiation as a test of the nature of X-ray radiation from the clusters of galaxies*, *Comments Astrophys. Space Phys.* **4** (1972) 173 [INSPIRE].

[45] A. Spacek et al., *Searching for Fossil evidence of AGN feedback in wise-selected stripe-82 galaxies by measuring the thermal Sunyaev–Zel'dovich effect with the Atacama Cosmology Telescope*, *Astrophys. J.* **834** (2017) 102 [arXiv:1610.02068] [INSPIRE].

[46] V. Vikram, A. Lidz and B. Jain, *A measurement of the galaxy-group thermal Sunyaev–Zel'dovich effect cross-correlation function*, *Mon. Not. Roy. Astron. Soc.* **467** (2017) 2315 [arXiv:1608.04160] [INSPIRE].

[47] H. Tanimura et al., *Probing hot gas around luminous red galaxies through the Sunyaev–Zel'dovich effect*, *Mon. Not. Roy. Astron. Soc.* **491** (2020) 2318 [arXiv:1903.06654] [INSPIRE].

[48] N. Koukoufilippas, D. Alonso, M. Bilicki and J.A. Peacock, *Tomographic measurement of the intergalactic gas pressure through galaxy–tSZ cross-correlations*, *Mon. Not. Roy. Astron. Soc.* **491** (2020) 5464 [arXiv:1909.09102] [INSPIRE].

[49] J. Meinke et al., *The thermal Sunyaev–Zel'dovich effect from massive, quiescent* $0.5 \leq z \leq 1.5$ *galaxies*, *Astrophys. J.* **913** (2021) 88 [*Erratum ibid.* **952** (2023) 170] [arXiv:2103.01245] [INSPIRE].

[50] Atacama Cosmology Telescope collaboration, *Atacama Cosmology Telescope: combined kinematic and thermal Sunyaev-Zel'dovich measurements from BOSS CMASS and LOWZ halos*, *Phys. Rev. D* **103** (2021) 063513 [arXiv:2009.05557] [INSPIRE].

[51] C.T. Pratt, Z. Qu and J.N. Bregman, *The resolved Sunyaev–Zel'dovich profiles of nearby galaxy groups*, *Astrophys. J.* **920** (2021) 104 [arXiv:2105.01123] [INSPIRE].

[52] Z. Yan et al., *Probing galaxy bias and intergalactic gas pressure with KiDS Galaxies-tSZ-CMB lensing cross-correlations*, *Astron. Astrophys.* **651** (2021) A76 [arXiv:2102.07701] [INSPIRE].

[53] A. Cooray and R.K. Sheth, *Halo models of large scale structure*, *Phys. Rept.* **372** (2002) 1 [astro-ph/0206508] [INSPIRE].

[54] F. van den Bosch et al., *Cosmological constraints from a combination of galaxy clustering and lensing — I. Theoretical framework*, *Mon. Not. Roy. Astron. Soc.* **430** (2013) 725 [arXiv:1206.6890] [INSPIRE].

[55] S. More et al., *The weak lensing signal and the clustering of BOSS galaxies II: astrophysical and cosmological constraints*, *Astrophys. J.* **806** (2015) 2 [arXiv:1407.1856] [INSPIRE].



JCAP10(2025)051

[56] DES and ACT collaborations, *Cross-correlation of Dark Energy Survey year 3 lensing data with ACT and Planck thermal Sunyaev-Zel'dovich effect observations. II. Modeling and constraints on halo pressure profiles*, *Phys. Rev. D* **105** (2022) 123526 [arXiv:2108.01601] [INSPIRE].

[57] S. Amodeo et al., *Atacama Cosmology Telescope: modeling the gas thermodynamics in BOSS CMASS galaxies from kinematic and thermal Sunyaev-Zel'dovich measurements*, *Phys. Rev. D* **103** (2021) 063514 [*Erratum ibid.* **107** (2023) 063514] [arXiv:2009.05558] [INSPIRE].

[58] E. Moser et al., *The impacts of modeling choices on the inference of circumgalactic medium properties from Sunyaev–Zeldovich observations*, *Astrophys. J.* **919** (2021) 2 [arXiv:2103.02469] [INSPIRE].

[59] E. Moser, N. Battaglia and S. Amodeo, *Searching for systematics in forward modeling Sunyaev-Zeldovich profiles*, arXiv:2307.10919 [INSPIRE].

[60] Z. Zheng et al., *Theoretical models of the halo occupation distribution: separating central and satellite galaxies*, *Astrophys. J.* **633** (2005) 791 [astro-ph/0408564] [INSPIRE].

[61] SDSS collaboration, *Galaxy clustering in the completed SDSS redshift survey: the dependence on color and luminosity*, *Astrophys. J.* **736** (2011) 59 [arXiv:1005.2413] [INSPIRE].

[62] DES collaboration, *Dark Energy Survey year 1 results: weak lensing mass calibration of redMaPPer galaxy clusters*, *Mon. Not. Roy. Astron. Soc.* **482** (2019) 1352 [arXiv:1805.00039] [INSPIRE].

[63] SDSS collaboration, *The clustering of luminous red galaxies in the Sloan Digital Sky Survey imaging data*, *Mon. Not. Roy. Astron. Soc.* **378** (2007) 852 [astro-ph/0605302] [INSPIRE].

[64] H. Guo et al., *The clustering of galaxies in the SDSS-III Baryon Oscillation Spectroscopic Survey: modelling of the luminosity and colour dependence in the data release 10*, *Mon. Not. Roy. Astron. Soc.* **441** (2014) 2398 [arXiv:1401.3009] [INSPIRE].

[65] H.S. Zhao, *Analytical models for galactic nuclei*, *Mon. Not. Roy. Astron. Soc.* **278** (1996) 488 [astro-ph/9509122] [INSPIRE].

[66] J.F. Navarro, C.S. Frenk and S.D.M. White, *A universal density profile from hierarchical clustering*, *Astrophys. J.* **490** (1997) 493 [astro-ph/9611107] [INSPIRE].

[67] N. Battaglia, J.R. Bond, C. Pfrommer and J.L. Sievers, *On the cluster physics of Sunyaev-Zel'dovich surveys I: the influence of feedback, non-thermal pressure and cluster shapes on Y-M scaling relations*, *Astrophys. J.* **758** (2012) 74 [arXiv:1109.3709] [INSPIRE].

[68] A. Kravtsov, A. Vikhlinin and A. Meshscheryakov, *Stellar mass-halo mass relation and star formation efficiency in high-mass halos*, *Astron. Lett.* **44** (2018) 8 [arXiv:1401.7329] [INSPIRE].

[69] R. Kou and J.G. Bartlett, *Cosmic census: relative distributions of dark matter, galaxies, and diffuse gas*, *Astron. Astrophys.* **675** (2023) A149 [arXiv:2211.07502] [INSPIRE].

[70] BOSS collaboration, *The eleventh and twelfth data releases of the Sloan Digital Sky Survey: final data from SDSS-III*, *Astrophys. J. Suppl.* **219** (2015) 12 [arXiv:1501.00963] [INSPIRE].

[71] PLANCK collaboration, *Planck 2018 results. VIII. Gravitational lensing*, *Astron. Astrophys.* **641** (2020) A8 [arXiv:1807.06210] [INSPIRE].

[72] PLANCK collaboration, *Planck 2015 results. XXII. A map of the thermal Sunyaev-Zeldovich effect*, *Astron. Astrophys.* **594** (2016) A22 [arXiv:1502.01596] [INSPIRE].

JCAP10(2025)051

[73] C. Maraston et al., *Stellar masses of SDSS-III BOSS galaxies at $z \sim 0.5$ and constraints to galaxy formation models*, *Mon. Not. Roy. Astron. Soc.* **435** (2013) 2764 [arXiv:1207.6114] [INSPIRE].

[74] N. Battaglia, J.R. Bond, C. Pfrommer and J.L. Sievers, *On the cluster physics of Sunyaev-Zel'dovich surveys II: deconstructing the thermal SZ power spectrum*, *Astrophys. J.* **758** (2012) 75 [arXiv:1109.3711] [INSPIRE].

[75] B. Bolliet et al., *class_sz I: overview*, *EPJ Web Conf.* **293** (2024) 00008 [arXiv:2310.18482] [INSPIRE].

[76] N. Sehgal et al., *The Atacama Cosmology Telescope: relation between galaxy cluster optical richness and Sunyaev-Zel'dovich effect*, *Astrophys. J.* **767** (2013) 38 [arXiv:1205.2369] [INSPIRE].

[77] DES collaboration, *Weak-lensing mass calibration of redMaPPer galaxy clusters in Dark Energy Survey science verification data*, *Mon. Not. Roy. Astron. Soc.* **469** (2017) 4899 [arXiv:1610.06890] [INSPIRE].

[78] E. Moser et al., *The circumgalactic medium from the CAMELS simulations: forecasting constraints on feedback processes from future Sunyaev–Zeldovich observations*, *Astrophys. J.* **933** (2022) 133 [arXiv:2201.02708] [INSPIRE].

[79] B. Diemer and A.V. Kravtsov, *Dependence of the outer density profiles of halos on their mass accretion rate*, *Astrophys. J.* **789** (2014) 1 [arXiv:1401.1216] [INSPIRE].

[80] DES collaboration, *Dark Energy Surveyed year 1 results: calibration of cluster mis-centring in the redMaPPer catalogues*, *Mon. Not. Roy. Astron. Soc.* **487** (2019) 2578 [arXiv:1901.07119] [INSPIRE].

[81] S. Yuan et al., *The DESI one-per cent survey: exploring the halo occupation distribution of luminous red galaxies and quasi-stellar objects with AbacusSummit*, *Mon. Not. Roy. Astron. Soc.* **530** (2024) 947 [arXiv:2306.06314] [INSPIRE].

[82] L. Linke et al., *KiDS+VIKING+GAMA: halo occupation distributions and correlations of satellite numbers with a new halo model of the galaxy-matter bispectrum for galaxy-galaxy-galaxy lensing*, *Astron. Astrophys.* **665** (2022) A38 [arXiv:2204.02418] [INSPIRE].

[83] I.G. McCarthy et al., *FLAMINGO: combining kinetic SZ effect and galaxy-galaxy lensing measurements to gauge the impact of feedback on large-scale structure*, arXiv:2410.19905 [INSPIRE].

[84] B. Hadzhiyska et al., *Evidence for large baryonic feedback at low and intermediate redshifts from kinematic Sunyaev-Zel'dovich observations with ACT and DESI photometric galaxies*, arXiv:2407.07152 [INSPIRE].

[85] BOSS collaboration, *The tenth data release of the Sloan Digital Sky Survey: first spectroscopic data from the SDSS-III Apache point observatory galactic evolution experiment*, *Astrophys. J. Suppl.* **211** (2014) 17 [arXiv:1307.7735] [INSPIRE].

[86] S. Saito et al., *Connecting massive galaxies to dark matter haloes in BOSS — I. Is galaxy colour a stochastic process in high-mass haloes?*, *Mon. Not. Roy. Astron. Soc.* **460** (2016) 1457 [arXiv:1509.00482] [INSPIRE].

[87] A. Leauthaud et al., *Lensing is low: cosmology, galaxy formation, or new physics?*, *Mon. Not. Roy. Astron. Soc.* **467** (2017) 3024 [arXiv:1611.08606] [INSPIRE].

[88] Simons Observatory collaboration, *The Simons Observatory: science goals and forecasts*, *JCAP* **02** (2019) 056 [arXiv:1808.07445] [INSPIRE].

JCAP10(2025)051

[89] CMB-S4 collaboration, *CMB-S4 science book, first edition*, (2016) [DOI:10.2172/1352047] [arXiv:1610.02743] [INSPIRE].

[90] DESI collaboration, *The DESI experiment part i: science, targeting, and survey design*, arXiv:1611.00036 [INSPIRE].

[91] S. Yuan, B. Hadzhiyska, S. Bose and D.J. Eisenstein, *Illustrating galaxy–halo connection in the DESI era with illustrisTNG*, *Mon. Not. Roy. Astron. Soc.* **512** (2022) 5793 [arXiv:2202.12911] [INSPIRE].

[92] S. Yuan et al., *The DESI one-per cent survey: exploring the halo occupation distribution of luminous red galaxies and quasi-stellar objects with AbacusSummit*, *Mon. Not. Roy. Astron. Soc.* **530** (2024) 947 [arXiv:2306.06314] [INSPIRE].

[93] A. Rocher et al., *The DESI one-percent survey: exploring the halo occupation distribution of emission line galaxies with AbacusSummit simulations*, *JCAP* **10** (2023) 016 [arXiv:2306.06319] [INSPIRE].

[94] A. Pillepich et al., *Simulating galaxy formation with the IllustrisTNG model*, *Mon. Not. Roy. Astron. Soc.* **473** (2018) 4077 [arXiv:1703.02970] [INSPIRE].

[95] D. Nelson et al., *First results from the IllustrisTNG simulations: the galaxy colour bimodality*, *Mon. Not. Roy. Astron. Soc.* **475** (2018) 624 [arXiv:1707.03395] [INSPIRE].

[96] J.P. Naiman et al., *First results from the IllustrisTNG simulations: a tale of two elements — chemical evolution of magnesium and europium*, *Mon. Not. Roy. Astron. Soc.* **477** (2018) 1206 [arXiv:1707.03401].

[97] F. Marinacci et al., *First results from the IllustrisTNG simulations: radio haloes and magnetic fields*, *Mon. Not. Roy. Astron. Soc.* **480** (2018) 5113 [arXiv:1707.03396] [INSPIRE].

[98] D. Nelson et al., *First results from the TNG50 simulation: galactic outflows driven by supernovae and black hole feedback*, *Mon. Not. Roy. Astron. Soc.* **490** (2019) 3234 [arXiv:1902.05554] [INSPIRE].

[99] R. Davé et al., *Simba: cosmological simulations with black hole growth and feedback*, *Mon. Not. Roy. Astron. Soc.* **486** (2019) 2827 [arXiv:1901.10203] [INSPIRE].

[100] E. Hernández-Martínez et al., *Cosmological and astrophysical parameter inference from stacked galaxy cluster profiles using CAMELS-zoomGZ*, *Astrophys. J.* **981** (2025) 170 [arXiv:2410.10942] [INSPIRE].

[101] CAMELS collaboration, *The CAMELS project: Cosmology and Astrophysics with MachinE Learning Simulations*, *Astrophys. J.* **915** (2021) 71 [arXiv:2010.00619] [INSPIRE].

[102] CAMELS collaboration, *The CAMELS multifield data set: learning the universe's fundamental parameters with artificial intelligence*, *Astrophys. J. Supp.* **259** (2022) 61 [arXiv:2109.10915] [INSPIRE].

JCAP10(2025)051